Journal of Advanced Research xxx (xxxx) xxx

Contents lists available at ScienceDirect

Journal of Advanced Research

journal homepage: www.elsevier.com/locate/jare

Original Article

Immune response and mesenchymal transition of papillary thyroid carcinoma reflected in ultrasonography features assessed by radiologists and deep learning

Jandee Lee [a,1], Jung Hyun Yoon [b,1], Eunjung Lee [c], Hwa Young Lee [a], Seonhyang Jeong [d], Sunmi Park [d], Young Suk Jo [d,*], Jin Young Kwak [b,*]

[a] Department of Surgery, Open NBI Convergence Technology Research Laboratory, Yonsei Cancer Center, Severance Hospital, Yonsei University College of Medicine, Seoul 03722, South Korea
[b] Department of Radiology, Severance Hospital, Research Institute of Radiological Science, Yonsei University, College of Medicine, Seoul 03722, South Korea
[c] School of Mathematics and Computing (Computational Science and Engineering), Yonsei University, Seoul 03722, South Korea
[d] Department of Internal Medicine, Open NBI Convergence Technology Research Laboratory, Yonsei University College of Medicine, Seoul 03722, South Korea

HIGHLIGHTS

- The suspicious ultrasonography features are related to immune response in thyroid cancer.
- The features were also related to epithelial to mesenchymal transition (EMT).
- Immune response and EMT were related to aggressive clinical behaviors.
- Immune response and EMT reflected in the decision by radiologists and convolutional neural networks.

GRAPHICAL ABSTRACT

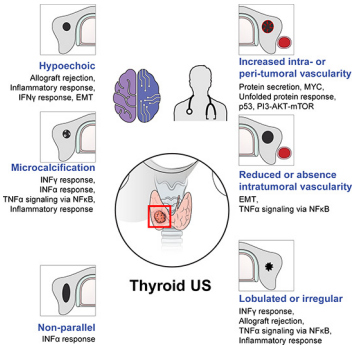

ARTICLE INFO

Article history:
Received 15 January 2023
Revised 7 September 2023
Accepted 29 September 2023
Available online xxxx

Keywords:
Ultrasonography
Papillary thyroid cancer
Transcriptome
Radiologists
Convolutional neural network
Immune response

ABSTRACT

Introduction: Ultrasonography (US) features of papillary thyroid cancers (PTCs) are used to select nodules for biopsy due to their association with tumor behavior. However, the molecular biological mechanisms that lead to the characteristic US features of PTCs are largely unknown.
Objectives: This study aimed to investigate the molecular biological mechanisms behind US features assessed by radiologists and three convolutional neural networks (CNN) through transcriptome analysis.
Methods: Transcriptome data from 273 PTC tissue samples were generated and differentially expressed genes (DEGs) were identified according to US feature. Pathway enrichment analyses were also conducted by gene set enrichment analysis (GSEA) and ClusterProfiler according to assessments made by radiologists and three CNNs - CNN1 (ResNet50), CNN2 (ResNet101) and CNN3 (VGG16). Signature gene scores for PTCs were calculated by single-sample GSEA (ssGSEA).
Results: Individual suspicious US features consistently suggested an upregulation of genes related to immune response and epithelial-mesenchymal transition (EMT). Likewise, PTCs assessed as positive by

Abbreviations: AI, Artificial intelligence; CNN, Convolutional neural network; DEG, Differentially expressed genes; EMT, Epithelial-mesenchymal transition; ERK, Extracellular signal-regulated kinase; FDR, False discovery rate; GSEA, Gene set enrichment analysis; LNM, Lymph node metastasis; PTC, Papillary thyroid cancers; SEER, Surveillance, Epidemiology, and End Results; TD, Thyroid differentiation; TF, Transcription factor; TIRADS, Thyroid Imaging and Reporting Data Systems; ETE, Extrathyroidal extension; TME, Tumor microenvironment; US, Ultrasonography.

* Corresponding authors.
E-mail addresses: joys@yuhs.ac (Y.S. Jo), docjin@yuhs.ac (J.Y. Kwak).
[1] These authors contributed equally to this work.

https://doi.org/10.1016/j.jare.2023.09.043
2090-1232/© 2023 Production and hosting by Elsevier B.V. on behalf of Cairo University..
This is an open access article under the CC BY-NC-ND license (http://creativecommons.org/licenses/by-nc-nd/4.0/).

Please cite this article as: J. Lee, J.H. Yoon, E. Lee et al., Immune response and mesenchymal transition of papillary thyroid carcinoma reflected in ultrasonography features assessed by radiologists and deep learning, Journal of Advanced Research, https://doi.org/10.1016/j.jare.2023.09.043

Epithelial-mesenchymal transition

radiologists and three CNNs showed the coordinate enrichment of similar gene sets with abundant immune and stromal components. However, PTCs assessed as positive by radiologists had the highest number of DEGs, and those assessed as positive by CNN3 had more diverse DEGs and gene sets compared to CNN1 or CNN2. The percentage of PTCs assessed as positive or negative concordantly by radiologists and three CNNs was 85.6% (231/273) and 7.1% (3/273), respectively.

Conclusion: US features assessed by radiologists and CNNs revealed molecular biologic features and tumor microenvironment in PTCs.

© 2023 Production and hosting by Elsevier B.V. on behalf of Cairo University.. This is an open access article under the CC BY-NC-ND license (http://creativecommons.org/licenses/by-nc-nd/4.0/).

Introduction

According to the Surveillance, Epidemiology, and End Results (SEER) Program, the incidence of thyroid cancers has nearly doubled in the past two decades [1], with consistently low death rates of 0.4 to 0.5%. This phenomenon has been attributed to the increased detection of small, clinically indolent, low-risk thyroid cancers [2–4]. Owing to the combination of increased number of cases and high detection rate, intense debates have taken place over "over-diagnosis" and "overtreatment" issues in the management of thyroid cancer [5–6]. Active surveillance has been introduced for low-risk thyroid cancers [7]. This management approach incorporates intense ultrasonography (US) monitoring for changes in size or feature. Newly detected regional cervical lymph nodes show features suspicious for metastasis [8]. Stringent management guidelines recommend the use of high resolution US to differentiate benign and malignant thyroid nodules and Thyroid Imaging Reporting And Data Systems [9–12]. US not only demonstrates superior differential diagnoses of thyroid nodules, but can also be used in the triage or monitoring of low-risk thyroid cancer candidates [13–15].

Individual US descriptors used for differential diagnosis have shown high sensitivity for thyroid cancers. Hypoechogenicity, defined as lower echogenicity compared to surrounding thyroid parenchyma, is a common US feature for papillary thyroid cancers (PTCs) [16]). Pathologically, microcalcifications (fine echogenic foci measuring less than 1 mm on US) correspond to concentric lamellated calcified structures known as psammoma bodies (PBs) [17]. PBs are common in PTC; however, they are detected even in non-neoplastic lesions, such as benign hyperplastic thyroid nodules and autoimmune thyroid diseases [17]. The pathogenesis of PBs was initially thought to be the dystrophic calcification of cancer cells [18]. Now, researchers propose PBs as products of a biologically active process driven by cancer cells [19]. Another US feature, related to PTCs, is the non-parallel shape (taller-than-wide), which is less sensitive but highly specific for malignancy [20]. Microlobulated, or irregular margins, with infiltrative tumor borders are most commonly found in PTCs and have been associated with epithelial-mesenchymal transition (EMT), and immune response [21].

However, the assessment of the abovementioned suspicious US features is largely dependent on who performs or interprets the US examination [22–23]. In addition, intratumoral heterogeneity is common in human cancers, and cytopathologic samples have limited value in representing heterogeneous characteristics within a tumor [24–25]. With the rapid evolution of computational technology and data processing, deep learning-based artificial intelligence (AI) has been applied to medical imaging, including thyroid US [26–30]. Based on quantitative data, deep learning-based AI is more objective and thus, may help overcome observer variability for a better representation of intratumoral heterogeneity. Although studies have attempted to link US features to pathologic findings, not many have done so with molecular biologic approaches. This is true specifically for differentially expressed genes (DEGs) that might be responsible for the characteristic US features of PTCs. Evaluating these associations may provide us with more accurate information that can be used to triage patients with low-risk cancers. This can be done in addition to qualitative US assessments performed by radiologists or quantitative AI data.

In this study, we generated transcriptome data using histologically proven PTC samples. We also investigated gene expression profiles based on US features that were assessed by radiologists and deep learning-based AI. The objective of our study was to understand the molecular mechanism underlying the US features that characterize thyroid cancers. Additionally, our goal was to gain deeper insight by comparing the similarities and dissimilarities regarding the decisions made by radiologists and deep learning-based AIs.

Materials and methods

Patients and specimens

Thyroid cancer and matched contralateral normal human tissue samples were obtained from 273 patients who went thyroidectomy for conventional PTC at the Yonsei Cancer Center (Seoul, South Korea) between May 2014 and January 2018. The diagnosis and evaluation of PTC were conducted in accordance with the guidelines of the American Thyroid Society and the Korean Thyroid Society [9]. All samples were frozen in liquid nitrogen and stored at −80 °C until use. Written informed consent was obtained from all patients in this study. The study protocol was approved by the Institutional Review Board of Yonsei Cancer Center, Severance Hospital (IRB-No. 4-2013-0546 and 4-2019-1487), Seoul, Korea.

Image acquisition and US assessment by radiologists

At our institution, preoperative staging US is performed in all patients before thyroid surgery. During the study period, these examinations were performed by one of the 23 radiologists (five staff radiologists with 3 to 25 years of experience in thyroid imaging and 18 fellows with 1 to 2 years of experience) who were dedicated to thyroid imaging. High frequency linear transducers (5 to 12 MHz) (*i*U22 or EPIQ 5, Philips Healthcare, Bothell, WA, USA) were used. During the staging examinations, individual US features of cancers were prospectively analyzed. Results for the following categories were recorded in our institutional database. Composition was classified as solid, predominantly solid (cystic portion < 50%), or predominantly cystic (cystic portion ≥50%). Echogenicity was classified as hyper-, iso-, hypoechoic (compared to the surrounding thyroid parenchyma) or marked hypoechoic (hypoechoic compared to the adjacent strap muscle). Margins were classified as circumscribed and non-circumscribed (microlobulated or irregular). Calcifications were classified as no calcifications, macro- or eggshell calcifications, microcalcifications, and mixed

calcifications. Shape was classified as parallel or non-parallel (taller-than-wide, greater in the anteroposterior dimension than the transverse dimension). Suspicious US features were marked hypoechogenicity, non-circumscribed margins, microcalcifications, and non-parallel shape. Vascularity was evaluated using 2D Doppler scans and classified into three patterns, i.e., reduced or absent vascularity (absence of Doppler signals within the thyroid nodule), peritumoral vascularity (presence of Doppler signals in the nodule's periphery), and intratumoral vascularity (presence of Doppler signals within the thyroid nodule despite peripheral vascularity). PTCs were assigned a "negative assessment" if there were no suspicious US features within the nodule, or a "positive assessment" if there were one or more suspicious US features [31].

Image analysis using deep learning-based artificial intelligence

Deep learning algorithms, such as CNNs, depend heavily on data size; i.e., the more data used for algorithm construction, the better the performance. Due to the limited amount of US image data, in-house deep learning-based AIs have been built through transfer learning using pre-trained deep CNNs [32]. These carefully designed and sophisticated CNNs were trained using more than a million images to maximize the accuracy of their results. Therefore, we retained the structure of these CNNs (transfer learning) and used other parameters as initial values for further modification (fine-tuning) with the US images. The fine-tuning process adjusts the provided parameter values, including weights and biases. This is done through an optimization process that uses a stochastic gradient descent with a momentum scheme to better fit a given US data set. The initial learning rate was set to 0.0003; 10–20 epochs were conducted and the last few layers were modified to agree with the number of binary classes for US features (benign and malignant). A total of 13,560 US images were collected for thyroid nodules at Severance Hospital from 2004 to 2019 (with IRB approval, IRB-No. 4-2019-0163) and were used to train the data in the fine-tuning process. The training set comprised representative US images of 7160 malignant and 6400 benign nodules confirmed cytopathologically. Randomly selected 760 benign images were augmented by left-right mirroring and added to the benign data set to balance the amount of data in each class. We fine-tuned 17 pre-trained CNNs, including GoogLeNet, Inception-v3 and Xception.

Representative images of thyroid cancer were selected for each case by one radiologist (J.Y.K.). The images were saved in the Picture Archiving and Communication System (PACS) as JPEG files. The Microsoft Paint program (version 6.1; Microsoft Corporation, Redmond, WA, USA) was used to outline square region-of-interests (ROIs) on the images to include the entire thyroid mass. Three fine-tuned convolutional neural networks (CNN) (ResNet50, ResNet101, and VGG16) among the seventeen CNNs were chosen to compare gene expression patterns among PTCs according to imaging features for their excellent sensitivity, specificity, and accuracy in image recognition tasks (refer to the Supplementary Materials and Methods for detailed information). ResNet50 is 50 layers deep and has 25.6 million parameters in the overall network [33]. The basic structure of T ResNet101 is similar; however, it is much deeper with 101 layers and 44.6 million parameters [34]. VGG16 has 16 layers with 138 million parameters [35]. For notational simplicity, ResNet50, ResNet101, and VGG16 were designated as convolution neural network (CCN) 1, 2, and 3, respectively. The three CNNs individually provided continuous malignancy risk scores (scale 0–100%) for each input of US images. Risk scores $\geq$50% defined a positive CNN assessment and scores <50% defined a negative assessment.

RNA extraction and sequencing

Total RNA was isolated from frozen tissues using the TRIzol reagent (Thermo Fisher Scientific, Waltham, MA, USA). RNA quality was assessed using a 2100 Bioanalyzer System (Agilent Technologies, Santa Clara, CA, USA). Next, the TruSeq Stranded mRNA LT Sample Prep Kit (Illumina, CA, USA) was used to prepare a cDNA library according to the sample preparation guide (Part #15031048 Rev E) by Macrogen Inc. (Seoul, Korea). NovaSeq 6000 (Illumina, San Diego, CA, USA) was used for 100 nt paired-end sequencing. To remove bias, low-quality RNA or artifacts, such as adaptor sequences, contaminant DNA, and PCR duplicates, were trimmed from the raw data. Trimmed data were mapped to the reference genome using HISAT2 (version 2.1.0) and aligned reads were generated. StringTie (version 2.1.3b) was used to reconstruct genes and estimate expressions using reference-based aligned read information. The transcripts were normalized to fragments per kilobase of transcript per million mapped reads (FPKM) and transcripts per million kilobases (TPM). Fold changes were calculated using the TPM Log2 value to analyze DEGs. Genes with fold changes >2 and *P*-values < 0.05 were used for the g:Profiler analysis (https://biit.cs.ut.ee/gprofiler) of significant terms related to gene ontology, pathways, and other gene function-related terms. To validate the results from high-throughput sequencing, quantitative real-time polymerase chain reaction (qRT-PCR) were performed (refer to the Supplementary Materials and Methods for detailed information).

GSEA and gProfiler

Genes identified as DEGs (fold changes >2 and two-tailed $P < 0.05$) were subjected to a functional enrichment analysis using the g:profiler2 (version 0.2.1) R package [36–37]. Gene Ontology (GO) biological process, GO cellular component, GO molecular function, Reactome, the Kyoto Encyclopedia of Genes and Genomes (KEGG), Hallmark GMT (MSigDB version 7.2) were used for functional enrichment analysis [38]. The significance threshold was met when gSCS < 0.05 and hypergeometric $P < 0.05$ were satisfied. Pathway enrichment analysis for DEGs was performed using ClusterProfiler, enrichplot, DOSE, ggplot2, org.Hs.eg.db R packages, and gene set enrichment analysis (GSEA) [39–40]. GO biological process, GO cellular component, GO molecular function and KEGG were used for pathway enrichment analysis using R. GSEA was performed using the hallmark gene set. The results were significant when $P < 0.05$ and FDRs < 0.25. The results were also presented using the Cnetplot to represent the linkages of genes and biological concepts.

Generation of the scoring system

We calculated signature scores by performing a single-sample GSEA (ssGSEA) using a signature gene set and estimating stromal and immune cells in malignant tumor tissues using expression data (ESTIMATE) R package (version 2.0.0) [41]. The calculated signature scores were stromal, immune, estimate, hallmark EMT, RAS, BRAF, extracellular signal-regulated kinase (ERK), and thyroid differentiation (TD) score [42]. ssGSEA was performed using transcriptome data from each of the 273 patients. The ESTIMATE score was calculated as the sum of the stromal and immune signature scores.

Statistical analysis

Continuous variables were compared using the two-tailed Student's *t*-test or the Mann–Whitney *U* test. Statistical analyses were performed with SPSS v.23.0 (IBM, Armonk, New York, USA) or

GraphPad Prism (GraphPad Software, San Diego, CA, USA). Data were presented as mean ± standard deviation (SD). Two-sided *P*-values < 0.05 were significant.

Results

Immune responses and EMT linked to individual suspicious US features assessed by radiologists

RNAseq was performed on tumor tissues from 273 patients with PTCs. The baseline clinicopathological and US features are summarized in Table 1. First, we performed a GSEA based on suspicious US features assessed by the radiologists to better understand molecular biological features. Genes related to immune response, such as for allograft rejection, inflammatory response, and IFN-γ were enriched in hypoechoic or marked hypoechoic PTCs compared to isoechoic PTCs (Fig. 1A). Furthermore, genes related to EMT, IL6-JAK-STAT3 signaling, and TNF-α signaling via NFκB were also enriched. EMT, IFN-γ response, IFN-α response, TNFα signaling via NFκB, inflammatory response, and allograft rejection were also highly enriched in PTCs with microcalcifications compared to PTCs without any types of calcification (Fig. 1B). Except for IFN-α response, the non-parallel shape was not associated with any significantly enriched gene set (Fig. 1C). Although other gene sets related to immune response were identified, they were not statistically significant. Similar patterns of gene enrichment with echogenicity or microcalcifications were also observed in microlobulated or irregular margins (Fig. 1D). Increased peritumoral and intratumoral vascularity was associated with genes involved in protein secretion, MYC, unfolded protein response, p53, and PI3-AKT-mTOR. (Fig. 2A). Reduced or absent vascularity was associated with genes related to EMT, allograft rejection and angiogenesis (Fig. 2B). GSEA of genes related to peritumoral vascularity did not reveal significant gene enrichment compared to those associated with reduced or absent vascularity. For absent vascularity, they were related to oxidative phosphorylation, E2F targets, and fatty acid metabolism (Fig. 2C). Comparative GSEA between intratumoral and reduced/absent vascularity revealed that intratumoral vascularity showed similar enriched genes sets to that of both peritumoral and intratumoral vascularity (Fig. 2D). Reduced or absent vascularity seemed to be related to EMT and TNFα signaling via NFκB. However, the q-values of the false discovery rate (FDR) were greater than 0.25. Both peritumoral and intratumoral vascularity did not have any gene sets that were differently expressed.

As our data indicated that suspicious US features were related to immune response, we calculated the stromal, immune, and estimate scores that reflect non-tumor cells in the tumor microenvironment (TME). Hypoechoic or marked hypoechoic PTCs showed higher stromal, immune and estimate scores compared to isoechoic PTCs (Supplementary Fig. 1A). PTCs with microcalcifications also showed higher stromal, immune and estimate scores compared to PTCs without calcification (Supplementary Fig. 1B). The non-parallel shape did not have statistically higher stromal, immune, and estimate scores compared to the parallel shape (Supplementary Fig. 1C). In contrast, microlobulated or irregular margins resulted in a statistically higher score compared to the circumscribed margin (Supplementary Fig. 1D). These results suggest that suspicious US features are tightly linked to non-tumor cells, such as fibroblasts and immune cells. To understand the biological characteristics of tumor cells, we also calculated EMT, RAS, BRAF, ERK, and TD scores. Notably, suspicious US features were related to aggressive tumorigenic molecular profiles, including higher EMT scores, lower RAS scores, higher BRAF and ERK scores, and lower TD scores (Supplementary Fig. 1A to 1D).

Table 1
Baseline characteristics of the 273 patients in the study population.

Clinicopathological features	n (%)
Age (years, mean ± SD)	49.8 ± 14.0
M:F (ratio)	67:206 (24.5:75.5)
Tumor size (cm)	1.8 ± 0.9 (0.5–7.8)
≤1/1 ~ 2/2–4/> 4 (cm)	40 (14.6)/163 (59.7)/63 (23.1)/7 (2.6)
Multifocality	
Single/Multiple/Bilateral	168 (61.5)/22 (8.1)/83 (30.4)
Microscopic extrathyroidal extension	218 (79.9)
T stage[α]	
T1/T2/T3/T4	47 (17.2)/9 (3.3)/190 (69.6)/27 (9.9)
N stage	
N0/N1a/N1b	90 (33.0)/80 (29.3)/103 (37.7)
M stage	271 (99.3)/2 (0.7)
M0/M1	
TNM stage[§]	
I/II/III/IV	76 (27.8)/3 (1.1)/115 (42.1)/79
Presence of BRAFV600E mutation	235 (86.1)
US features assessed by radiologists	n (%)
Composition (solid/predominantly solid/predominantly cystic)	255 (93.4)/18 (6.6)/0 (0.0)
Echogenicity (hyper-/iso-/hypo-/markedly hypoechoic)	0 (0.0)/18 (6.6)/212 (77.7)/43 (15.7)
Margins (well/microlobulated/irregular)	31 (11.4)/153 (56.0)/89 (32.6)
Calcifications (no calcification/macro- or eggshell/micro-/mixed)	93 (34.1)/35 (12.8)/114 (41.7)/31 (11.4)
Shape (parallel/non-parallel)	146 (53.5)/127 (46.5)
Vascularity (no/intratumoral/peritumoral/both)	101 (37.0)/17 (6.2)/96 (35.2)/59 (21.6)
Echotexture (heterogeneous/homogeneous) echogenicity)	60 (22.0)/213 (78.0)
Final assessment (Negative/Positive)	14 (5.1)/259 (94.9)
Malignancy risk score (range, 0–100%, mean ± SD) of CNN	
CNN1	91.4 ± 15.9
CNN2	87.3 ± 22.3
CNN3	85.6 ± 21.7
Decisions made by CNN (Negative/Positive)	n (%)
CNN1	13 (4.8)/260 (95.2)
CNN2	24 (8.8)/249 (91.2)
CNN3	24 (8.8)/249 (91.2)

Abbreviations: TNM, TNM Classification of Malignant Tumors 8th edition; SD, standard deviation; CNN, convolutional neural network.

Prediction of gene expression changes based on the final radiological assessment

DEGs were evaluated based on binary assessments provided by the radiologists. Positive PTCs showed 2,147 upregulated and 209 downregulated genes, indicating diverse gene expression changes (Supplementary Figs. 2 and 3). GSEA with hallmark gene sets included those with individual suspicious US features, such as IFN-γ response, allograft rejection, inflammatory response, TNFα signaling via NFκB, INFα response, IL6-JAK-STAT3 signaling, and EMT. Furthermore, genes sets associated with the p53 pathway and the mitotic spindle were enriched in positive PTCs in addition to those with individual suspicious US features (Fig. 3A). Our calculations also indicated higher stromal, immune, estimate, EMT, BRAF, and ERK scores and lower RAS and TD scores (Fig. 3B and Supplementary Fig. 4). Based on g:Profiler, diverse immune-related gene sets were identified for GO biological processes, cellular component, and molecular function. Reactome gene set analysis also identified immune-related gene sets and proto-oncogenic transcription factors, such as MYC, AML1, and c-JUN. These genes were listed as candidate transcription factors (TFs) for suspicious US features of PTC (Fig. 3C, 3D, and Supplementary Table 1).

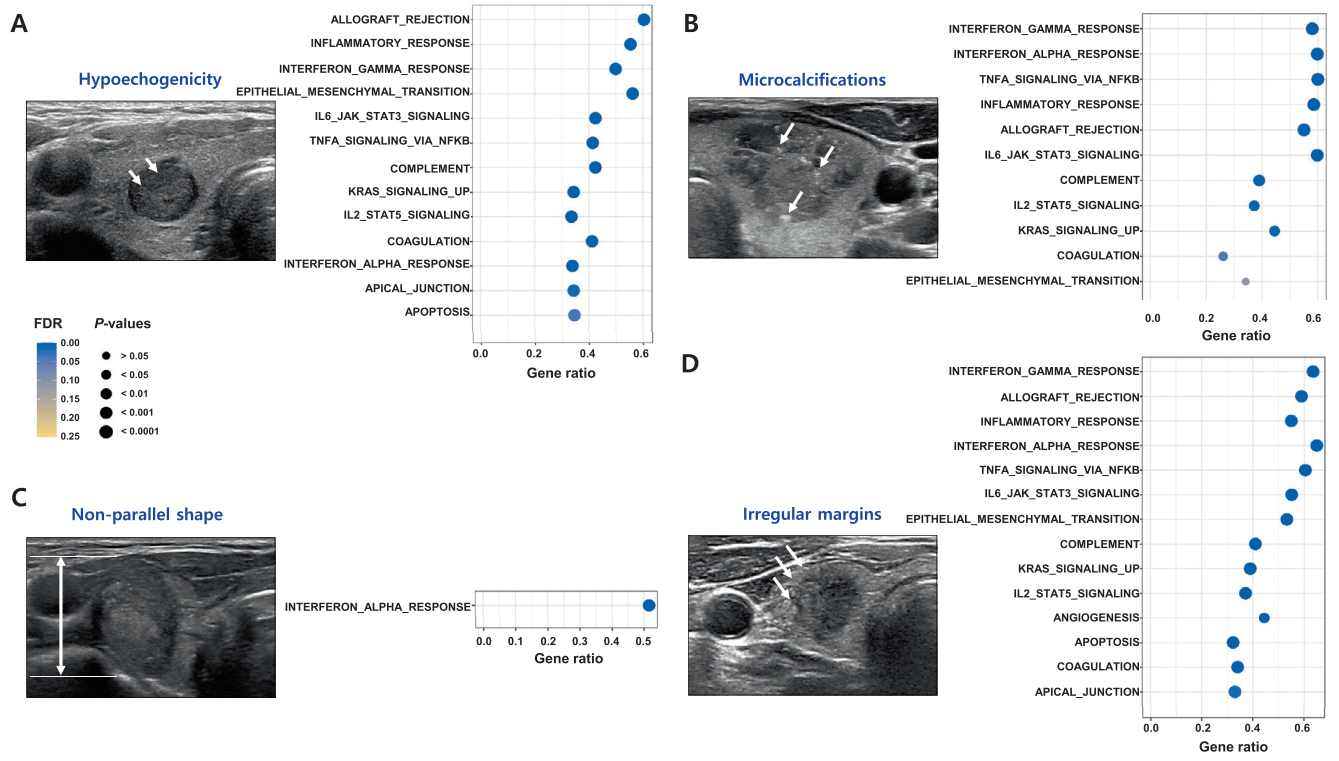

Fig. 1. Representative images and dot plots for the GSEA results according to the US features assessed by radiologists. **A-D**. Images and GSEA present gene sets enriched in hypoechoic or marked hypoechoic PTCs (n = 255) compared to isoechoic PTCs (n = 18) (A), PTCs with microcalcification (n = 114) compared to PTCs without calcifications (n = 93) (B), PTCs with non-parallel shape (n = 127) compared to PTCs with parallel shape (n = 146) (C), and PTCs with microlobulated or irregular margins (n = 242) compared to PTCs with circumscribed margins (n = 31) (D). Abbreviations: GSEA, gene set enrichment analysis: FDR, false discovery rate.

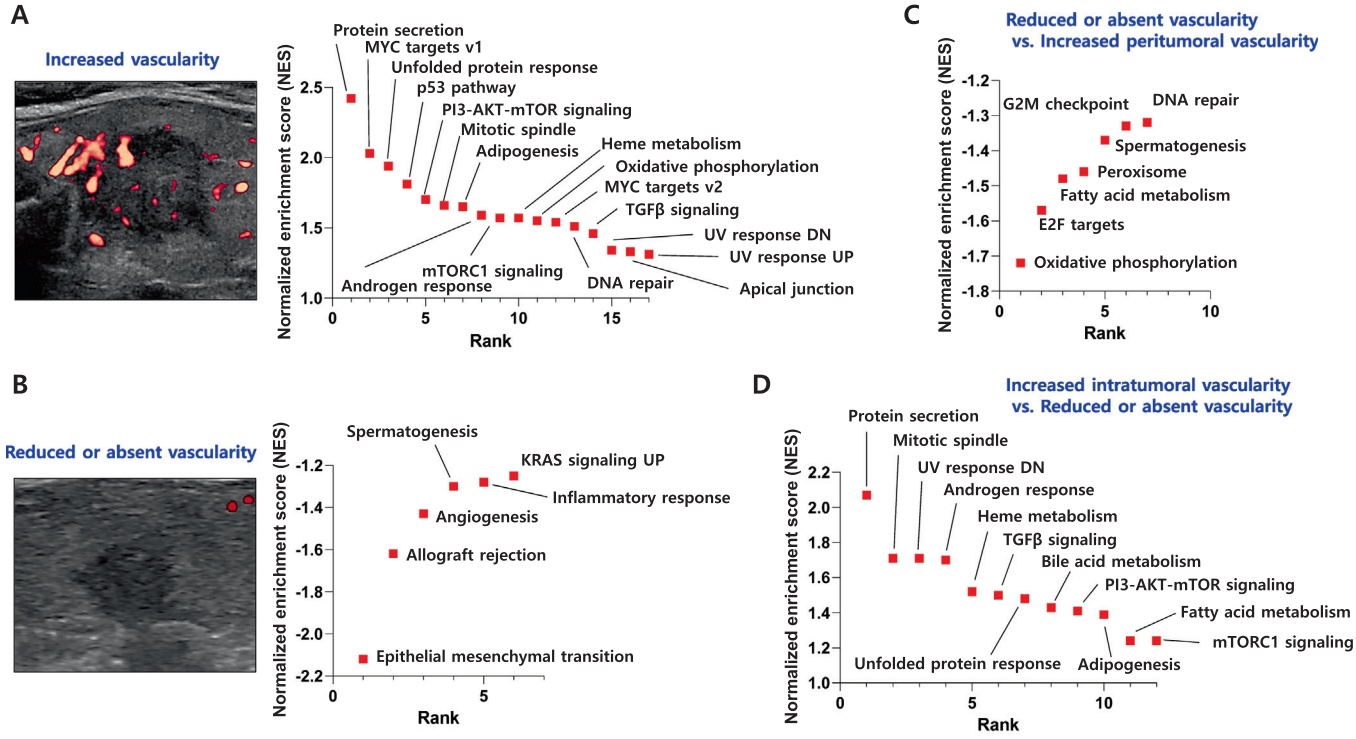

Fig. 2. GSEA results based on the presence of vascularity on US. **A** and **B**. GSEA represents gene sets enriched in PTCs with increased (peritumoral and intratumoral) vascularity (n = 172) (A) and PTCs with reduced or absent vascularity (n = 101) (B). **C**. GSEA represents gene sets enriched in PTCs with reduced or absent vascularity (n = 101) compared to PTCs with increased peritumoral vascularity (n = 96). **D**. GSEA represents gene sets enriched in PTCs with increased intratumoral vascularity (n = 17) compared to PTCs with reduced or absent vascularity (n = 101). Abbreviations: GSEA, gene set enrichment analysis.

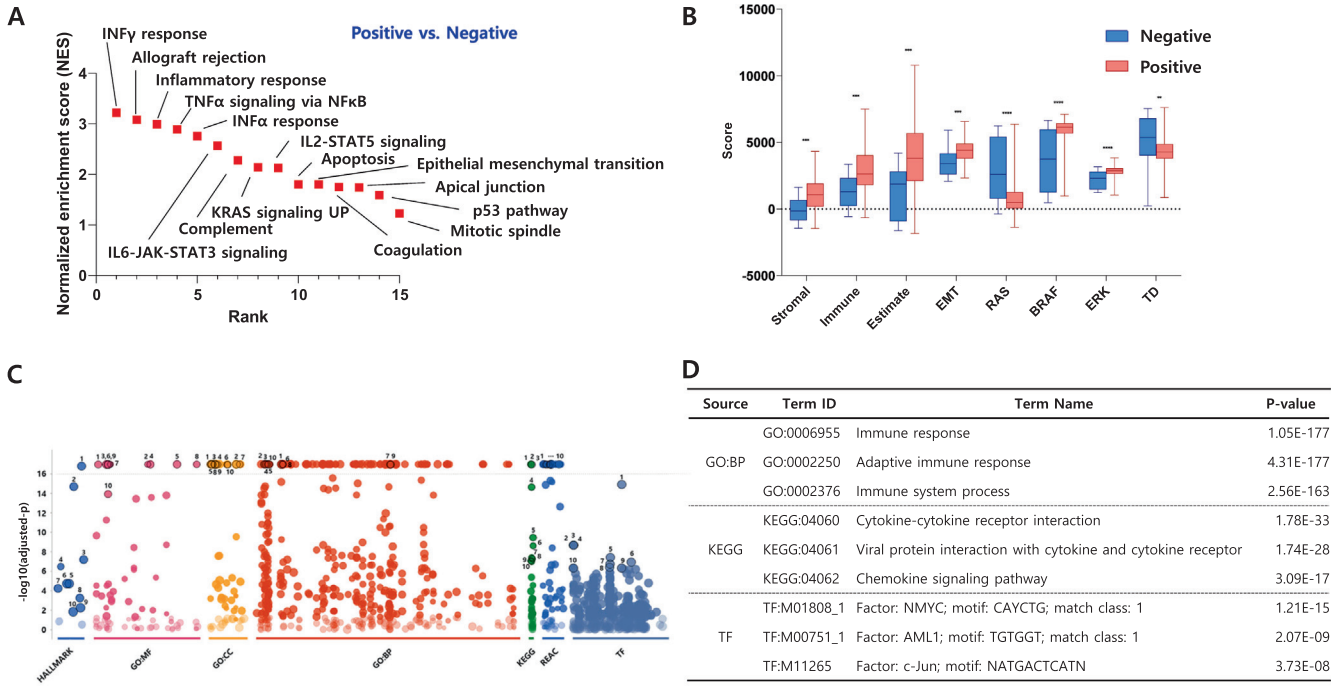

Source	Term ID	Term Name	P-value
GO:BP	GO:0006955	Immune response	1.05E-177
	GO:0002250	Adaptive immune response	4.31E-177
	GO:0002376	Immune system process	2.56E-163
KEGG	KEGG:04060	Cytokine-cytokine receptor interaction	1.78E-33
	KEGG:04061	Viral protein interaction with cytokine and cytokine receptor	1.74E-28
	KEGG:04062	Chemokine signaling pathway	3.09E-17
TF	TF:M01808_1	Factor: NMYC; motif: CAYCTG; match class: 1	1.21E-15
	TF:M00751_1	Factor: AML1; motif: TGTGGT; match class: 1	2.07E-09
	TF:M11265	Factor: c-Jun; motif: NATGACTCATN	3.73E-08

Fig. 3. Molecular biological characteristics according to binary decisions made by radiologists using US images. **A**. GSEA using hallmark gene sets represent coordinately enriched gene sets in PTCs assessed as positive (n = 259) compared to those assessed as negative (n = 14) by radiologists on US. These gene sets met the following criteria: FDR q-value < 0.25, nominal *P*-value < 0.05. **B**. Comparison of molecular scores between PTCs assessed as negative and positive on US. The box extended from the 25th to 75th percentiles, and the whiskers indicated all points. *P*-values were calculated using the Mann–Whitney *U* test. *** *P*-value < 0.001, **** *P*-value < 0.0001. **C**. g:Profiler results using differentially- expressed genes (DEGs, fold changes > 2 and two-tailed *P*-values < 0.05). The figure depicts the gene sets enriched in PTCs assessed as positive on US; the number indicates the ranking for each group from the Molecular Signatures Database (MSigDB; HALLMARK, GO:MF, GO:CC, GO:BP, KEGG, REAC, and TF). For detailed gene set names and statistical analysis results, refer to Supplementary Table 1. **D**. Representative gene sets related to Fig. 4C. Abbreviations: EMT, epithelial-mesenchymal transition; TD, thyroid differentiation; FDR, false discovery rate; MF, molecular function; CC, cellular component; BP, biological process; KEGG, Kyoto Encyclopedia of Genes and Genomes; REAC, Reactome; TF, transcription factor.

Diverse gene expression changes related to the final evaluations of interpreting radiologists and CNNs

To understand molecular features based on decisions made by CNNs, we first developed DEGs. CNN1 revealed 1135 upregulated and 38 downregulated genes (Supplementary Fig. 5). GSEA identified genes related to EMT, angiogenesis, and inflammatory response that were enriched in PTCs assessed as positive by CNN1 (Supplementary Fig. 6A). However, due to the small number of DEG and enriched gene sets, no signaling pathways relating to the IFN response, IL6-JAK-STAT3 signaling, and TNFα signaling via NFκB were identified. Furthermore, PTCs with positive CNN1 results had higher stromal, EMT, and BRAF scores and lower RAS scores (Supplementary Fig. 6B). DEG analysis for CNN2 identified 649 upregulated and 184 downregulated genes (Supplementary Fig. 7). As CNN2 also had a few DEGs, the score comparison for the GSEA and CNN1 were similar (Supplementary Fig. 8A and 8B). Unlike CNN1, PTCs assessed as positive by CNN2 had genes related to the IFN response and IL6-JAK-STAT3 signaling. PTCs assessed as positive by CNN3 had 1567 upregulated and 187 downregulated genes (Supplementary Fig. 9). Once again, the number of DEGs was small, and the GSEA results were similar to genes related to the immune response and EMT (Supplementary Fig. 10A). Except for the ERK score, the score comparison analysis for CNN3 revealed results similar to the assessments by the radiologists (Supplementary Fig. 10B). However, when the major TFs were analyzed, the radiologists and three CNNs revealed subtle differences (Fig. 4 and Supplementary Table 2 to 4).

The radiologists and CNN1 reported 14 and 13 false-negative cases, respectively. In contrast, CNN2 and CNN3 assessed 24 false-negative cases each (Fig. 5A). To understand the common molecular biological characteristics defined by the radiologists and CNNs, we compared the cases simultaneously evaluated as negative (n = 3, Fig. 5A) or positive (n = 231, Fig. 5B) by radiologists and CNNs 1–3. The three cases assessed as negative by radiologists and all CNNs included genes related to metabolism and synthesis, such as oxidative phosphorylation, fatty acid metabolism, adipogenesis, reactive oxygen species, glycolysis, and TORC1 signaling (Fig. 5C). In the 231 PTCs that were assessed as positive by the radiologists and CNNs, genes related to EMT and immune response were enriched and compatible with our GSEA for suspicious US features (Fig. 5D).

Discussion

In this study, we investigated the molecular biological features of pathologically-proven PTCs. These molecular features are the fundamental cause of US features considered suspicious by radiologists and deep learning-based AI [12]. Using RNA sequencing and in silico analysis, we identified TME as an important player in determining the characteristics of US images. GSEA performed according to echogenicity and tumor margin revealed that diverse immune responses, and EMT gene sets were highly enriched in PTCs, that had hypoechogenicity, microlobulated, or irregular margins. The presence of microcalcifications was related to immune responses and EMT; the non-parallel shape was also related to immune responses, despite the few statistically significant gene sets. GSEA according to vascular features presented somewhat different results. Increased vascularity, especially intratumoral vascularity, was associated with gene sets related to secretion, proliferation, replication, and synthesis. The immune responses and EMT were linked to decreased or absent vascularity.

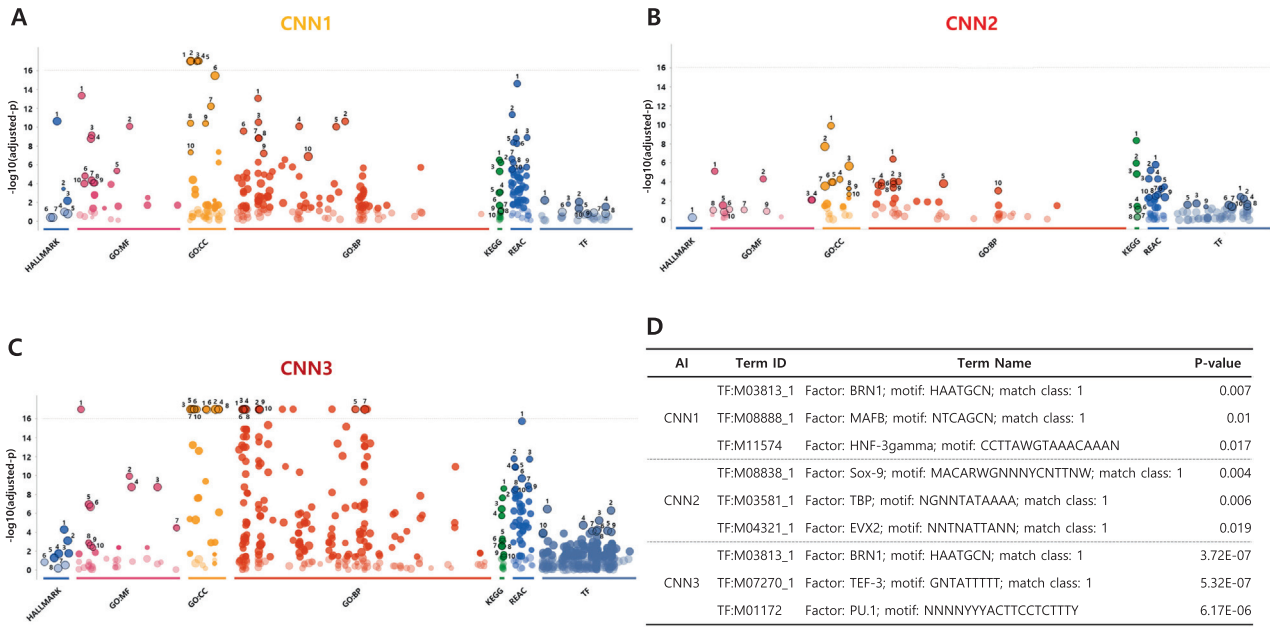

D

AI	Term ID	Term Name	P-value
CNN1	TF:M03813_1	Factor: BRN1; motif: HAATGCN; match class: 1	0.007
	TF:M08888_1	Factor: MAFB; motif: NTCAGCN; match class: 1	0.01
	TF:M11574	Factor: HNF-3gamma; motif: CCTTAWGTAAACAAAN	0.017
CNN2	TF:M08838_1	Factor: Sox-9; motif: MACARWGNNNYCNTTNW; match class: 1	0.004
	TF:M03581_1	Factor: TBP; motif: NGNNTATAAAA; match class: 1	0.006
	TF:M04321_1	Factor: EVX2; motif: NNTNATTANN; match class: 1	0.019
CNN3	TF:M03813_1	Factor: BRN1; motif: HAATGCN; match class: 1	3.72E-07
	TF:M07270_1	Factor: TEF-3; motif: GNTATTTTT; match class: 1	5.32E-07
	TF:M01172	Factor: PU.1; motif: NNNNYYYACTTCCTCTTTY	6.17E-06

Fig. 4. Molecular biological characteristics according to binary decisions made by the three CNNs. **A-C**. g:Profiler results are depicted using differentially expressed genes (DEGs, fold changes > 2 and two-tailed *P*-values < 0.05) according to CNN1, CNN2, and CNN3, respectively. Figures show gene sets enriched in PTCs with positive CNN results; the number indicates the ranking for each group from the Molecular Signatures Database (MSigDB; HALLMARK, GO:MF, GO:CC, GO:BP, KEGG, REAC, and TF). For detailed gene set names and statistical analysis results, refer to Supplementary Table 2 to 4. **D**. Representative transcription factor targets are related to Fig. 2A to 2C.

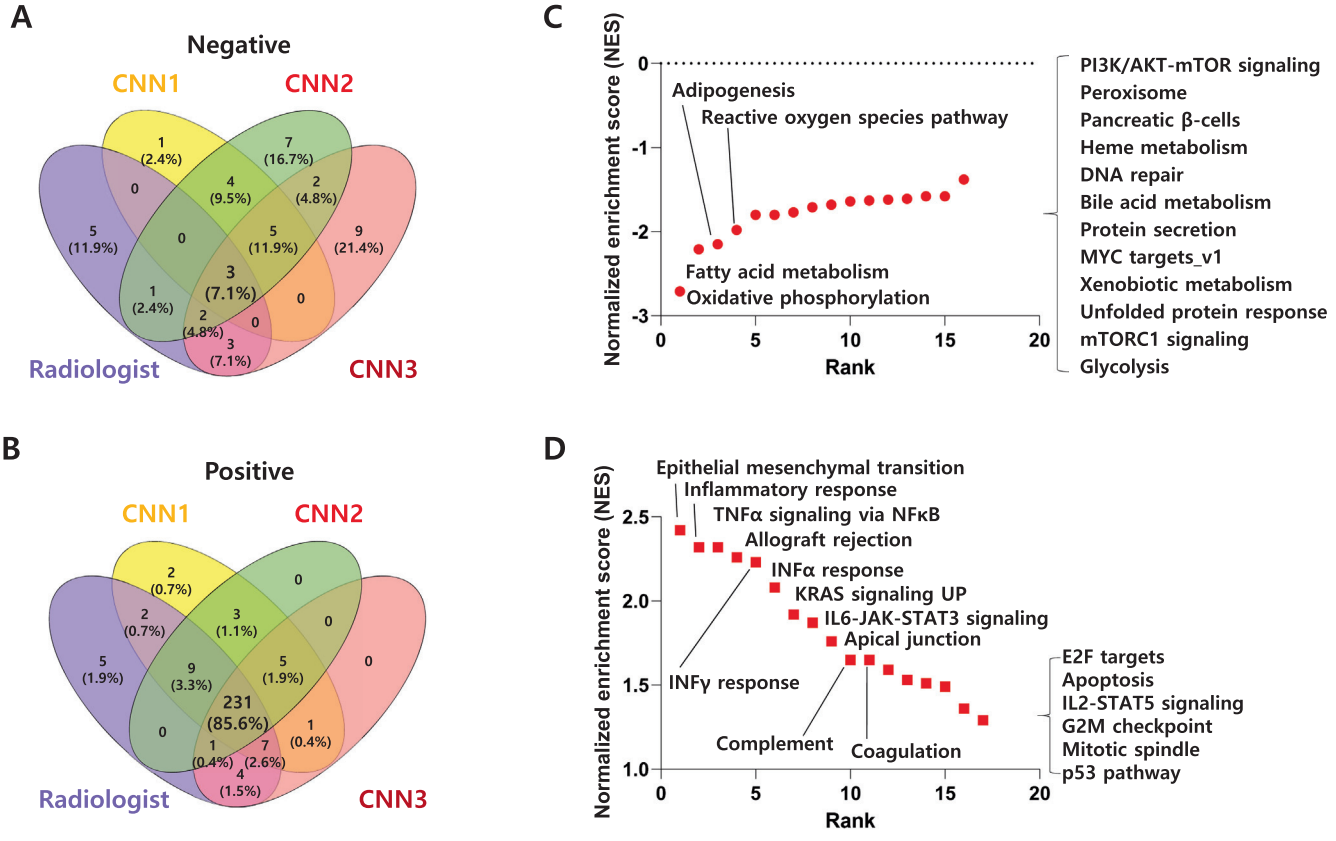

Fig. 5. Molecular biological characteristics according to the binary decisions of radiologists and three CNNs. **A** and **B**. A Venn diagram that presents the number of cases commonly assessed as negative or positive by radiologists and three CNNs. **C** and **D**. GSEA using hallmark gene sets presents gene sets highly enriched in nodules assessed as negative (C) or positive (D). Abbreviations: GSEA, gene set enrichment analysis.

Angiogenesis-related gene sets were also enriched in PTCs with low or no vascularity, indicating this vascular feature may be related to hypoxia. In contrast, increased vascularity may be related to oxidative phosphorylation, representing aerobic metabolism [43–46]. These findings suggest that suspicious US features are primarily related to TME and EMT, and that vascularity also reflects tumor metabolism status.

In regard to driver mutations, our samples showed a high frequency of the BRAFV600E mutation [235 (86.1%) out of 273 cases] as seen in previous reports in South Korea [47–48]. Molecular classification of TCGA THCA divided PTC into two representative groups; RAS-like and BRAF-like [42]. However, with the recent introduction of new research technology such as single cell transcriptome analysis, understanding of TME has deepened and tumor heterogeneity is no longer a complete mystery [49]. Even though the frequency of the BAFV600E mutation was higher in positive PTCs assessed by the radiologists and three CNNs (data not shown), our study shows relatively homogenous driver genes, but different BRAF, RAS, EMT, ERK and TD scores that reflect the characteristics of tumors, suggesting that additional tumor evolution to BRAFV600E is an important step leading to the ultrasonography features analyzed.

We performed the GSEA according to ETE and LNM to better understand the clinicopathological significance of TME and EMT (data not shown). Immune response-related signaling was also found in ETE-related gene sets. LNM-related gene sets were more diverse; besides the immune response and EMT gene sets, genes involved in TGF-β and NOTCH signaling were also enriched in PTCs with LNM [50–53]. The GSEA findings demonstrate that suspicious US features can be related to ETE, an aggressive clinical feature of PTCs. However, a more diverse or intense EMT was required for LNM that may not be reflected in the used suspicious US features [54–57]. This trend was also observed in the three CNNs. The diverse EMT-related gene sets identified in PTCs using LNM were not significantly documented in PTCs and were assessed as being positive by the three CNNs.

When comparing the assessments of the radiologists and three CNNs, gene sets related to TME and EMT were identified by both as positive PTCs. The cases assessed as positive by radiologists also had the highest number of DEGs. In contrast, those assessed as positive by CNN3, using VGG16, had more diverse DEGs and gene sets compared to CNNs that used ResNet50 and ResNet101, respectively. Based on the number of DEGs and identified gene sets, CNN3-determined features were more similar to US features determined by the radiologists. However, the number of PTCs in which cancer was misdiagnosed as benign tumors was the highest in CNN3 (n = 9), followed by radiologists (n = 5), CNN1 (n = 1), and CNN2 (n = 7). The subsequent GSEA suggested that the gene enrichment patterns observed in false-negative cases assessed by radiologists differed from those assessed by the three CNNs. For example, dysregulation of the cell cycle was neglected in false-negative cases assessed by radiologists. In contrast. both dysregulation of the cell cycle and MYC transactivation were not detected by CNN3. Of note, one false-negative case among CNN1 assessments was observed in which the number of DEGs was lower than that observed by radiologists and other CNNs. The differences in the identification of molecular characteristics amongst CNNs reflect the basis on which each algorithm was built. The three CNNs detected molecular characteristics differentially based on their pre-trained algorithms. Based on our research at this stage, it seems difficult to conclude which of these CNNs is superior. Further follow-up studies will be needed to understand and analyze the characteristics of each AI-based algorithm.

Primarily, this study was designed to evaluate gene expression related to characteristic US features seen in PTCs. Therefore, DEGs were investigated by comparing PTC samples, rather than comparing PTCs with benign thyroid nodules, as we anticipate future studies will. No definitive precancerous lesions of PTC were identified, limiting this comparative analysis [58–59]. Second, our data suggested that the more prominent the ultrasonography features, the more active the epithelial-mesenchymal transition was. However, not all signaling pathways that contribute to carcinogenesis may lead to the characteristic features seen on ultrasonography images by the naked eye or AI. For example, certain oncogenic signaling related to EMT (i.e., NOTCH signaling) is not reflected through US features. Furthermore, other hallmarks of cancer, such as metabolic remodeling, protein synthesis, dysregulation of the cell cycle, MYC transactivation, and hormone response, do not appear strongly as suspicious imaging features. The effects of the gene sets identified in this study on tumor progression must be further elucidated [42,60]. Third, one of the 23 radiologists independently assessed the US features of PTCs in the prospective collection of image data. The inherent subjectivity of the US assessments may have affected the results, but this was not considered in this study [22]. Last, the samples for this study were obtained from a single institution and the number of samples was limited. Therefore, subgroup analyses, such as the analysis performed according to gender (no difference between males and females in ultrasonography features), may have insufficient statistical power. Our findings need to be validated in larger multicenter studies with wet Lab-based validation experiments.

In summary, the composition of TME and aggressive PTC features were related to individual suspicious US features of PTCs. When applying three deep learning-based CNNs, scores calculated by CNN1 were generally similar to those calculated by radiologists. Distinct molecular features including TME characteristics and aggressive features were identified in PTCs assessed as positive by radiologists, and CNN algorithms identified various molecular characteristics according to the type of pre-trained algorithm (Supplementary Figure 11). US features assessed by radiologists and AI-based CNN can potentially predict the molecular biologic behaviors of PTCs.

Compliance with Ethics Requirements

All procedures followed were in accordance with the ethical standards of the responsible committee on human experimentation (Institutional Review Board of Yonsei Cancer Center, Severance Hospital, Seoul, Korea.) and with the Helsinki Declaration of 1975, as revised in 2008 (5). Informed consent was obtained from all patients for being included in the study.

Ethics approval and consent to participate

Written informed consent was obtained from all patients enrolled this study. The study protocol was approved by the Institutional Review Board of Yonsei Cancer Center, Severance Hospital (IRB-No. 4-2013-0546, 4-2019-0163 and 4-2019-1487), Seoul, Korea.

Consent for publication

Not applicable.

Data availability statement

The datasets generated during and/or analyzed during this study are available from the corresponding author on request.

Funding

We received funding from the National Research Foundation of Korea (NRF) funded by the Korean government: NRF-2018R1A2B6004179, NRF-2021R1H1A2012035 (Y.S.J.), NRF-2021R1A2C2007492 (J.Y.K.), NRF-2020R1A2C1006047 (J.L.), and NRF-2018R1C1B6006064 (J.H.Y.).

CRediT authorship contribution statement

Jandee Lee: Conceptualization, Investigation, Visualization, Funding acquisition, Writing – original draft, Writing – review & editing. **Jung Hyun Yoon:** Conceptualization, Visualization, Funding acquisition, Writing – original draft, Writing – review & editing. **Eunjung Lee:** Methodology, Investigation. **Hwa Young Lee:** Methodology, Investigation, Visualization. **Seonhyang Jeong:** Methodology. **Sunmi Park:** Methodology, Investigation, Supervision. **Young Suk Jo:** Conceptualization, Funding acquisition, Writing – review & editing. **Jin Young Kwak:** Conceptualization, Funding acquisition, Supervision, Writing – review & editing.

Declaration of Competing Interest

The authors declare that they have no known competing financial interests or personal relationships that could have appeared to influence the work reported in this paper.

Acknowledgments

The authors would like to thank Ji Young Kim and Hee Chang Yu, for their excellent technical support. The authors also thank Medical Illustration & Design, part of the Medical Research Support Services of Yonsei University College of Medicine, for all artistic support related to this work.

Appendix A. Supplementary data

Supplementary data to this article can be found online at https://doi.org/10.1016/j.jare.2023.09.043.

References

[1] Surveillance, Epidemiology, and End Result Program (SEER) Database 2022 [Available from: https://seer.cancer.gov/statfacts/html/thyro.html.
[2] Nambron R, Rosenthal R, Bahl D. Diagnosis and Evaluation of Thyroid Nodules-the Clinician's Perspective. Radiol Clin North Am 2020;58(6):1009–18.
[3] Genere N, El Kawkgi OM, Giblon RE, Vaccarella S, Morris JC, Hay ID, et al. Incidence of Clinically Relevant Thyroid Cancers Remains Stable for Almost a Century: A Population-Based Study. Mayo Clin Proc 2021;96(11):2823–30.
[4] Jeon MJ, Kim HK, Kim EH, Kim ES, Yi HS, Kim TY, et al. Decreasing Disease-Specific Mortality of Differentiated Thyroid Cancer in Korea: A Multicenter Cohort Study. Thyroid 2018;28(9):1121–7.
[5] Ahn HS, Kim HJ, Welch HG. Korea's thyroid-cancer "epidemic"–screening and overdiagnosis. N Engl J Med 2014;371(19):1765–7.
[6] Zaridze D, Maximovitch D, Smans M, Stilidi I. Thyroid cancer overdiagnosis revisited. Cancer Epidemiol 2021;74:102014.
[7] Ito Y, Uruno T, Nakano K, Takamura Y, Miya A, Kobayashi K, et al. An observation trial without surgical treatment in patients with papillary microcarcinoma of the thyroid. Thyroid 2003;13(4):381–7.
[8] Saravana-Bawan B, Bajwa A, Paterson J, McMullen T. Active surveillance of low-risk papillary thyroid cancer: A meta-analysis. Surgery 2020;167(1):46–55.
[9] Haugen BRM, Alexander EK, Bible KC, Doherty G, Mandel SJ, Nikiforov YE, et al. 2015 American Thyroid Association Management Guidelines for Adult Patients with Thyroid Nodules and Differentiated Thyroid Cancer. Thyroid 2015.
[10] Russ G, Royer B, Bigorgne C, Rouxel A, Bienvenu-Perrard M, Leenhardt L. Prospective evaluation of thyroid imaging reporting and data system on 4550 nodules with and without elastography. Eur J Endocrinol/Eur Federation Endocrine Soc 2013;168(5):649–55.
[11] Tessler FN, Middleton WD, Grant EG, Hoang JK, Berland LL, Teefey SA, et al. ACR Thyroid Imaging, Reporting and Data System (TI-RADS): White Paper of the ACR TI-RADS Committee. J Am Coll Radiol 2017;14(5):587–95.
[12] Ha EJ, Chung SR, Na DG, Ahn HS, Chung J, Lee JY, et al. 2021 Korean Thyroid Imaging Reporting and Data System and Imaging-Based Management of Thyroid Nodules: Korean Society of Thyroid Radiology Consensus Statement and Recommendations. Korean J Radiol 2021;22(12):2094–123.
[13] Gweon HM, Son EJ, Kim JA, Youk JH. Predictive Factors for Active Surveillance of Subcentimeter Thyroid Nodules with Highly Suspicious US Features. Ann Surg Oncol 2017;24(6):1540–5.
[14] Ghai S, O'Brien C, Goldstein DP, Sawka AM. Ultrasound in active surveillance for low-risk papillary thyroid cancer: imaging considerations in case selection and disease surveillance. Insights Imaging 2021;12(1):130.
[15] Rozenbaum A, Buffet C, Bigorgne C, Royer B, Rouxel A, Bienvenu M, et al. Outcomes of active surveillance of EU-TIRADS 5 thyroid nodules. Eur J Endocrinol/Eur Federation Endocrine Soc 2021;184(5):677–86.
[16] Smith-Bindman R, Lebda P, Feldstein VA, Sellami D, Goldstein RB, Brasic N, et al. Risk of thyroid cancer based on thyroid ultrasound imaging characteristics: results of a population-based study. JAMA Intern Med 2013;173(19):1788–96.
[17] Triggiani V, Guastamacchia E, Licchelli B, Tafaro E. Microcalcifications and psammoma bodies in thyroid tumors. Thyroid 2008;18(9):1017–8.
[18] Kubota T, Sato K, Yamamoto S, Hirano A. Ultrastructural study of the formation of psammoma bodies in fibroblastic meningioma. J Neurosurg 1984;60(3):512–7.
[19] Das DK. Psammoma body: a product of dystrophic calcification or of a biologically active process that aims at limiting the growth and spread of tumor? Diagn Cytopathol 2009;37(7):534–41.
[20] Shin JH, Baek JH, Chung J, Ha EJ, Kim JH, Lee YH, et al. Ultrasonography Diagnosis and Imaging-Based Management of Thyroid Nodules: Revised Korean Society of Thyroid Radiology Consensus Statement and Recommendations. Korean J Radiol 2016;17(3):370–95.
[21] Lee WK, Lee J, Kim H, Lee SG, Choi SH, Jeong S, et al. Peripheral location and infiltrative margin predict invasive features of papillary thyroid microcarcinoma. Eur J Endocrinol/Eur Federation Endocrine Soc 2019;181(2):139–49.
[22] Hoang JK, Middleton WD, Farjat AE, Teefey SA, Abinanti N, Boschini FJ, et al. Interobserver Variability of Sonographic Features Used in the American College of Radiology Thyroid Imaging Reporting and Data System. AJR Am J Roentgenol 2018;211(1):162–7.
[23] Sych YP, Fadeev VV, Fisenko EP, Kalashnikova M. Reproducibility and Interobserver Agreement of Different Thyroid Imaging and Reporting Data Systems (TIRADS). Eur Thyroid J 2021;10(2):161–7.
[24] Marusyk A, Almendro V, Polyak K. Intra-tumour heterogeneity: a looking glass for cancer? Nat Rev Cancer 2012;12(5):323–34.
[25] Fan M, Xia P, Clarke R, Wang Y, Li L. Radiogenomic signatures reveal multiscale intratumour heterogeneity associated with biological functions and survival in breast cancer. Nat Commun 2020;11(1):4861.
[26] Giger ML. Machine Learning in Medical Imaging. J Am Coll Radiol. 2018;15(3 Pt B):512-20.
[27] Hamet P, Tremblay J. Artificial intelligence in medicine. Metab Clin Exp 2017;69s:S36–s40..
[28] Ko SY, Lee JH, Yoon JH, Na H, Hong E, Han K, et al. Deep convolutional neural network for the diagnosis of thyroid nodules on ultrasound. Head Neck 2019;41(4):885–91.
[29] Koh J, Lee E, Han K, Kim EK, Son EJ, Sohn YM, et al. Diagnosis of thyroid nodules on ultrasonography by a deep convolutional neural network. Sci Rep 2020;10(1):15245.
[30] Li H, Weng J, Shi Y, Gu W, Mao Y, Wang Y, et al. An improved deep learning approach for detection of thyroid papillary cancer in ultrasound images. Sci Rep 2018;8(1):6600.
[31] Kim EK, Park CS, Chung WY, Oh KK, Kim DI, Lee JT, et al. New sonographic criteria for recommending fine-needle aspiration biopsy of nonpalpable solid nodules of the thyroid. AJR Am J Roentgenol 2002;178(3):687–91.
[32] Zhang J, Gao Z, Yin J, Quon MJ, Ye J. S6K directly phosphorylates IRS-1 on Ser270 to promote insulin resistance in response to TNF-α signaling through IKK2. J Biol Chem 2008.
[33] He K, Zhang X, Ren S, Sun J. Deep Residual Learning for Image Recognition. IEEE Conference on Computer Vision and Pattern Recognition (CVPR) 2016:770-8.
[34] Zaugg K, Yao Y, Reilly PT, Kannan K, Kiarash R, Mason J, et al. Carnitine palmitoyltransferase 1C promotes cell survival and tumor growth under conditions of metabolic stress. Genes Dev 2011;25(10):1041–51.
[35] Simonyan K, Zisserman A. Very deep convolutional networks for large-scale image recognition. arXiv 14091556. 2014.
[36] Subramanian A, Tamayo P, Mootha VK, Mukherjee S, Ebert BL, Gillette MA, et al. Gene set enrichment analysis: a knowledge-based approach for interpreting genome-wide expression profiles. Proc Natl Acad Sci U S A 2005;102(43):15545–50.
[37] Kolberg L, Raudvere U, Kuzmin I, Vilo J, Peterson H. gprofiler2 – an R package for gene list functional enrichment analysis and namespace conversion toolset g:Profiler. F1000Res. 2020;9.
[38] Mootha VK, Lindgren CM, Eriksson KF, Subramanian A, Sihag S, Lehar J, et al. PGC-1alpha-responsive genes involved in oxidative phosphorylation are

coordinately downregulated in human diabetes. Nat Genet 2003;34 (3):267–73.
[39] Yu G, Wang LG, Han Y, He QY. clusterProfiler: an R package for comparing biological themes among gene clusters. OMICS 2012;16(5):284–7.
[40] Yu G, Wang LG, Yan GR, He QY. DOSE: an R/Bioconductor package for disease ontology semantic and enrichment analysis. Bioinformatics 2015;31 (4):608–9.
[41] Yoshihara K, Shahmoradgoli M, Martinez E, Vegesna R, Kim H, Torres-Garcia W, et al. Inferring tumour purity and stromal and immune cell admixture from expression data. Nat Commun 2013;4:2612.
[42] . Cell 2014;159(3):676–90.
[43] Solaini G, Sgarbi G, Baracca A. Oxidative phosphorylation in cancer cells. Biochim Biophys Acta 2011;1807(6):534–42.
[44] Ashton TM, McKenna WG, Kunz-Schughart LA, Higgins GS. Oxidative Phosphorylation as an Emerging Target in Cancer Therapy. Clin Cancer Res 2018;24(11):2482–90.
[45] Hapke RY, Haake SM. Hypoxia-induced epithelial to mesenchymal transition in cancer. Cancer Lett 2020;487:10–20.
[46] Saxena K, Jolly MK, Balamurugan K. Hypoxia, partial EMT and collective migration: Emerging culprits in metastasis. Transl Oncol 2020;13(11):100845.
[47] Jo YS, Li S, Song JH, Kwon KH, Lee JC, Rha SY, et al. Influence of the BRAF V600E mutation on expression of vascular endothelial growth factor in papillary thyroid cancer. J Clin Endocrinol Metab 2006;91(9):3667–70.
[48] Lee SE, Hwang TS, Choi YL, Kim WY, Han HS, Lim SD, et al. Molecular Profiling of Papillary Thyroid Carcinoma in Korea with a High Prevalence of BRAF (V600E) Mutation. Thyroid 2017;27(6):802–10.
[49] Pu W, Shi X, Yu P, Zhang M, Liu Z, Tan L, et al. Single-cell transcriptomic analysis of the tumor ecosystems underlying initiation and progression of papillary thyroid carcinoma. Nat Commun 2021;12(1):6058.
[50] Yamashita AS, Geraldo MV, Fuziwara CS, Kulcsar MA, Friguglietti CU, da Costa RB, et al. Notch pathway is activated by MAPK signaling and influences papillary thyroid cancer proliferation. Transl Oncol 2013;6(2):197–205.
[51] Lee J, Seol MY, Jeong S, Kwon HJ, Lee CR, Ku CR, et al. KSR1 is coordinately regulated with Notch signaling and oxidative phosphorylation in thyroid cancer. J Mol Endocrinol 2015;54(2):115–24.
[52] Choi D, Ramu S, Park E, Jung E, Yang S, Jung W, et al. Aberrant Activation of Notch Signaling Inhibits PROX1 Activity to Enhance the Malignant Behavior of Thyroid Cancer Cells. Cancer Res 2016;76(3):582–93.
[53] Garcia-Rendueles AR, Rodrigues JS, Garcia-Rendueles ME, Suarez-Farina M, Perez-Romero S, Barreiro F, et al. Rewiring of the apoptotic TGF-beta-SMAD/NFkappaB pathway through an oncogenic function of p27 in human papillary thyroid cancer. Oncogene 2017;36(5):652–66.
[54] Lee JM, Dedhar S, Kalluri R, Thompson EW. The epithelial-mesenchymal transition: new insights in signaling, development, and disease. J Cell Biol 2006;172(7):973–81.
[55] Kalluri R, Weinberg RA. The basics of epithelial-mesenchymal transition. J Clin Invest 2009;119(6):1420–8.
[56] Acloque H, Adams MS, Fishwick K, Bronner-Fraser M, Nieto MA. Epithelial-mesenchymal transitions: the importance of changing cell state in development and disease. J Clin Invest 2009;119(6):1438–49.
[57] Lamouille S, Xu J, Derynck R. Molecular mechanisms of epithelial-mesenchymal transition. Nat Rev Mol Cell Biol 2014;15(3):178–96.
[58] Frank R, Baloch ZW, Gentile C, Watt CD, LiVolsi VA. Multifocal fibrosing thyroiditis and its association with papillary thyroid carcinoma using BRAF pyrosequencing. Endocr Pathol 2014;25(3):236–40.
[59] Canberk S. Precursor and borderline lesions of the thyroid (indolent lesions of epithelial origin): from theory to practice. Gland Surg 2020;9(5):1724–34.
[60] Xing M. Recent advances in molecular biology of thyroid cancer and their clinical implications. Otolaryngol Clin North Am 2008;41(6):1135–46. ix.